Quantum Electronics **32** (7) 570 – 586 (2002)

INVITED PAPER

PACS numbers: 28.60.+s; 32.80.-t; 42.55.-f
DOI: 10.1070/QE2002v032n07ABEH002250

Some new trends in laser isotope separation in atomic vapours*

P.A. Bokhan, V.V. Buchanov, D.E. Zakrevskii, M.A. Kazaryan,
M.M. Kalugin, A.M. Prokhorov, N.V. Fateev

Contents

1. Introduction **570**
2. Laser facility for isotope separation **571**
3. Coherent isotope-selective two-photon excitation **572**
3.1. Brief description of two-photon excitation and its mathematical model
3.2. Two-photon excitation of lead atoms
3.3. Two-photon excitation of boron and silicon atoms
4. Photochemical separation of zinc isotopes using two-photon excitation **576**
4.1. Description of the method
4.2. Polarisation of radiation
4.3. Mathematical model of cascade superluminescence
4.4. Results of calculations
4.5. Experimental results
5. Photochemical isotope separation using one-photon excitation of long-lived levels **580**
5.1. Experimental method
5.2. Mathematical model
5.3. Calculations on separation of zinc isotopes
5.4. Experiments on separation of zinc isotopes
5.5. Separation of rubidium isotopes by exciting Rydberg states
6. Conclusions **584**
References **585**

***Abstract*. New approaches to the methods of laser isotope separation are considered and realised which substantially extend the possibilities of the methods. To narrow down an absorption line and decrease parasitic absorption at transitions in isotope atoms that do not belong to an isotope being separated, two-photon excitation of atoms was used both in collinear and counterpropagating light beams. By using two-photon excitation in counterpropagating light beams, the weight amounts of Zn isotopes were separated under the conditions when the isotopic structure of a resonance transition was completely masked by the Doppler broadening. Two-photon excitation in collinear beams was used for efficient purification of lead from a rare ^{210}Pb isotope to obtain a low-radioactive lead. A detailed computer simulation of separation of isotopes of Zn, B, Pb, and Si using two-photon excitation was performed. An efficient method of isotope separation involving chemical reactions with selectively excited long-lived atoms was proposed and realised. The method offers some advantages over the conventional photoionisation method.**

Keywords: *laser isotope separation, two-photon excitation, photochemistry.*

*The main results of this work were reported and discussed 19 November 2001 at a seminar of the Department of Oscillations, General Physics Institute, RAS, headed by A.M. Prokhorov.

P.A. Bokhan, D.E. Zakrevskii, N.V. Fateev Institute of Semiconductor Physics, Siberian Branch, Russian Academy of Sciences, prosp. akad. Lavrent'eva 13, 630090 Novosibirsk, Russia;
V.V. Buchanov 'Astrofisika' Research and Production Association, Volokolamskoe sh. 95, 123424 Moscow, Russia;
M.A. Kazaryan P.N. Lebedev Physics Institute, Russian Academy of Sciences, Leninskii prosp. 53, 119991 Moscow, Russia;
M.M. Kalugin Scanning Lasers Enterprise, ul. Leningradskaya 16-29, 188537 Sosnovyi Bor, Leningradskaya oblast, Russia;
A.M. Prokhorov A.M. Prokhorov General Physics Institute, Russian Academy of Sciences, ul. Vavilova 38, 119991 Moscow, Russia

Received 25 January 2002
Kvantovaya Elektronika **32** (7) 570 – 586 (2002)
Translated by M.N. Sapozhnikov

1. Introduction

Today, one can assert that isotopic products and ultra-pure substances play an increasing role in science, technology, and medicine. Therefore, it is not surprising that a search for new methods of isotope separation is being continued and already known methods are being rapidly improved.

Laser methods of isotope separation and purification of substances [1–3] in atomic vapours have been developed for several decades [4–15]. The experimental facilities have been built (as early as 1975, a setup based on a dye laser pumped by a self-heated copper vapour laser [16–18] was used at the Lawrence Livermore National Laboratory to obtain a weight amount of enriched uranium with the concentration of ^{235}Ur of about 3 % [15, 19, 20]), as well as pilot–plant and industrial units [21–33].

The qualitative development of the laser equipment occurring in the last decade due to the creation of efficient and high-power tunable lasers in the visible, UV, and IR spectral regions [34–43] gives grounds to expect a technological break in the building of industrial laser units for isotope separation. The versatility of a laser method for separating different isotopes and the possibility of separating a required element with a high degree of purity from natural ore, industrial alloys or waste products are very important in this case.

Successful laser separation of isotopes of uranium, plutonium, gadolinium, zirconium, and ytterbium has been reported in Refs [13, 15, 22–25]. This field of research is being extensively developed in USA, France, and Japan, where large-scale production of isotopes can be expected in the near future [13–15]. This technology also attracts interest in Great Britain, India, China, Republic of Korea, and some other countries, including Russia [14, 15, 31, 44, 45].

In this paper, we present the results of theoretical and experimental studies on laser separation of isotopes of some elements (Pb, Zn, Rb, B, Si), which can be used in fundamental studies for creating quantum computers, as well as in microelectronic, atomic, and biomedicine technologies [32, 33, 44, 45].

On the one hand, the choice of elements considered in this paper was determined by the requirements of science and technology. First of all, this concerns lead and silicon, which are widely used in microelectronics. On the other hand, our choice was determined in some cases by the potential possibilities of the modern laser equipment [10, 11, 22–25, 38, 43, 46–49] and by competitiveness of laser methods compared to other methods such as centrifugal separation and isotopic chemical exchange.

In this paper, we focus our attention on physicochemical aspects of isotope separation and, to a lesser degree, on the development of laser technology. The high power and high efficiency of modern copper vapour and dye lasers, as well as tunable crystal lasers, especially diode-pumped Nd^{3+}:YAG lasers [50] make it possible to organise the economical production of isotopes if laser radiation is used efficiently.

2. Laser unit for isotope separation

A laser unit for isotope separation [48, 49] (Fig. 1), which allows one to study excitation of vapours of various substances using a variety of schemes and excitation conditions, consists of two independent laser channels, each of which emitting at its own wavelength.

Master oscillators. Tunable coherent radiation is produced by organic dye lasers (as a rule, rhodamine 6G lasers) [51] pumped by a 10-W cw argon laser. The output power of tunable lasers at 607 and 615 nm amounts to 70 mW.

The laser resonator contained three selective elements: a three-component birefrigent filter, a Fabry–Perot etalon, and a Troitsky film. An electronic control unit provided

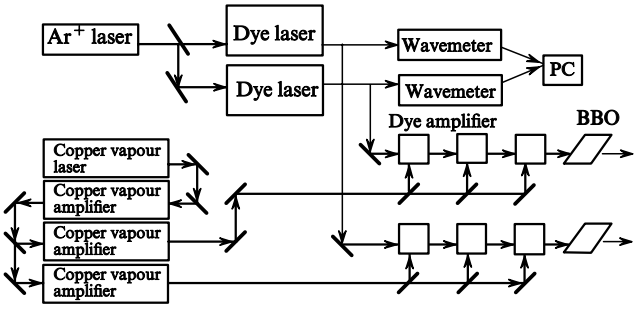

Figure 1. Optical block diagram of the setup.

single-frequency lasing. The output spectrum was controlled with the help of a scanning Fabry–Perot interferometer. Accurate measurements of the width of the spectrum (from the beat spectrum of two identical lasers) showed that the width of the emission line was smaller than 5 MHz during measurements for a few seconds, while the frequency drift was several hundreds of megahertz per hour. The central emission frequency of each of the lasers was controlled with a wavemeter. The relative error of measurements was 5×10^{-8}, but the absolute error was 150–200 MHz due to imperfect calibration and the temperature drift (about 100 MHz h^{-1}).

Radiation from each of the master lasers was amplified with a three-stage pulsed amplifying system consisting of cells transversely pumped by a copper vapour laser. The distance between master lasers and preamplifiers was ~ 10 m, which provided a weak effect of spontaneous radiation of amplifiers on cw lasers.

Unit of pump lasers. The unit of pump lasers consists of a master oscillator-power amplifier system based on copper vapour gas-discharge lasers including a master oscillator, a preamplifier, and two final amplifying stages. The water-cooled lasers were mounted in a single vertical module. In lasers, commercial Kristall sealed-off tubes (Istok State Research and Production Enterprise) [43] with the diameter of a discharge cannel of 20 mm and lengths 930 and 1230 mm were used (LT-30Cu or GL-202 tubes were used in a master oscillator, and an LT-40Cu tube was used in amplifiers). The master oscillator with an unstable resonator produced radiation with a nearly diffraction-limited divergence.

Copper lasers were excited by pulsed power supplies, in which a scheme with a partial discharge of a storage capacitance was used [49]. GMI-29A-1 generator vacuum tubes were used as switches (the commuted current achieved 280 A, the power was 5 kW, and the duration of an excitation pulse was ~ 50 ns). The storage capacitance was charged from a stabilised voltage transformer operating at a frequency of 30 kHz and the output voltage up to 30 kV.

The average power of the master oscillator was ~ 15 W for the output-pulse duration of 6–7 ns, which was insufficient for a complete removal of inversion in the preamplifier. The duration of the master oscillator pulse was increased up to ~ 15 ns with the help of a stretcher at the average output power of the preamplifier of 6–7 W, the output power of the preamplifier being increased almost by 30 %. For the input power at the preamplifier of ~ 6 W, the output power was ~ 55 W, and the overall output power in

the diffraction-limited beam after two amplifying channels of the copper vapour laser unit was no less than ~ 150 W (75 W in each channel at the output pulse repetition rate of $10-12$ kHz and the output pulse duration of $\sim 18-20$ ns for the average output power of the rectifier equal to ~ 4.5 kW). Because the output pulse was very short, the pulses fed to the master oscillator and amplifier were synchronised with an accuracy better than 0.5 ns and shifted relative to each other by the time for which light propagated from the master oscillator to the amplifier.

The operating parameters and working regimes of the unit were controlled with the help of a computer control system.

Pulsed dye amplifiers. Pulsed dye amplifiers also represent a two-channel system, each of the channels consisting in turn of three stages. A solution of dye phenalemine-512 in ethanol was used in all amplifying stages, which allowed the use of both emission lines of a copper laser with almost the same efficiency. The distance between the walls of cells in preamplifiers and final amplifiers was 0.5 and 1 mm, respectively. The pump radiation was focused to a cell by a cylindrical lens and then was reflected back from a cylindrical mirror. The dye concentration was chosen to provide the pump radiation transmission equal to 30 % per passage. This ensured a high (~ 90 %) utilisation of pump radiation and its uniform distribution.

To suppress amplified spontaneous emission, dispersion prisms were used together with a slit diaphragm and a lens telescope with a 0.2-mm diaphragm in the waist. In addition, delays between the amplified and pump pulses were carefully adjusted. The optimal delay was $\sim 1-2$ ns. The optimal gain of the first preamplifier was 10^4, which provided the output power of ~ 50 mW at the pump power of 10 W. The output power after the second amplifier was ~ 450 mW for the pump power of 12 W. The output power after the final stage was 12 W for the pump power of 48 W. The output emission had an almost Gaussian distribution.

System for radiation frequency doubling. UV radiation was obtained by doubling the output from a dye laser with the help of a nonlinear crystal. Radiation from dye amplifiers was focused into a BBO crystal of length 7 mm by a lens with a focal distance of 8.5 cm. The crystal was placed at a distance of 40 cm from the centre of a cell of the output stage. The output power of dye lasers was 12 W in the wavelength range from 600 to 615 nm, which allowed us to obtain the 9-ns second harmonic pulses at 307.6 and 303.6 nm with the average power of 3 W in each channel with a nearly Gaussian spatial distribution.

The unit of tunable lasers, together with the frequency-doubling system, provides emission of very narrow emission lines. In our case, the limiting theoretical width of a 10-ns output pulse after a final dye amplifier is $\Delta\nu_1 \approx (2\pi\tau)^{-1} = 16$ MHz, and the width of the second harmonic pulse is $\Delta\nu_2 = 2\Delta\nu_1 \approx 32$ MHz. The experimental width of the second harmonic was of about 50 MHz.

The spectral and energy characteristics of the laser unit were well maintained and reproduced during prolong continuous operation (up to 100 h). This allowed us to produce isotopes in weight amounts during physical studies.

3. Coherent isotope-selective two-photon excitation of atoms

3.1 Brief description of two-photon excitation and its mathematical model

Isotope separation was earlier performed, as a rule, by photoionisation with a sequence of incoherent one-photon transitions. This method was discussed in many papers and was considered in detail in review [14]. Upon two-photon excitation of atoms through an intermediate level, a transition to the final state occurs due to simultaneous absorption of two photons, when the intermediate level is weakly populated. The efficient two-photon isotope separation was achieved due to the recent improvement of the laser equipment [52–55].

A general scheme of two-photon excitation of atoms is shown in Fig. 2. It is characterised by the detuning Δ of a resonance frequency and the deviation δ of sum of radiation frequencies from an exact two-photon resonance (hereafter, simply the deviation δ). The optimum value of deviation is nonzero [56].

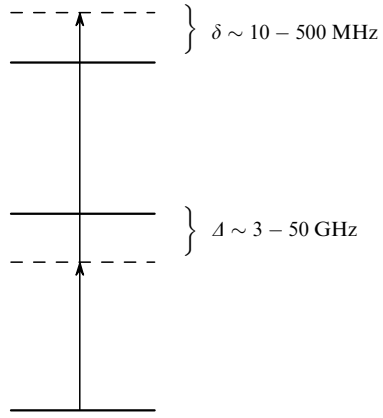

Figure 2. Scheme for two-photon excitation of atoms.

Upon excitation of atoms by short pulses (when the transverse relaxation time is comparable with the pulse duration or greater) with a narrow spectral width (comparable with the inverse pulse duration), the interaction of radiation with atoms should be described in the coherent approximation. According to the theoretical model [57], the dynamics of a three-level system can be described with the help of a density matrix. Equations for the elements of the density matrix in real variables for a three-level scheme of an atom in electromagnetic linearly polarised fields have the form [56]

$$\frac{\mathrm{d}}{\mathrm{d}t}\rho_{11} = -2\mu_1 V_1 + A_{21}\rho_{22},$$

$$\left(\frac{\mathrm{d}}{\mathrm{d}t} + \frac{1}{T_2}\right)\rho_{22} = 2(\mu_1 V_1 - \mu_2 V_2) + A_{32}\rho_{33},$$

$$\left(\frac{\mathrm{d}}{\mathrm{d}t} + \frac{1}{T_2} + W_3\right)\rho_{33} = 2\mu_2 V_2,$$

$$\left(\frac{\mathrm{d}}{\mathrm{d}t}+\frac{1}{2T_2}\right)u_1 = -\Omega_1\mu_1 - \mu_3 V_2,$$

$$\left(\frac{\mathrm{d}}{\mathrm{d}t}+\frac{1}{2T_2}\right)\mu_1 = \Omega_1 u_1 + V_1(\rho_{11}-\rho_{22}) + V_2 u_3, \qquad (1)$$

$$\left(\frac{\mathrm{d}}{\mathrm{d}t}+\frac{1}{2T_2}+\frac{1}{2T_3}+\frac{W_3}{2}\right)u_2 = -\Omega_2\mu_2 - \mu_3 V_1,$$

$$\left(\frac{\mathrm{d}}{\mathrm{d}t}+\frac{1}{2T_2}+\frac{1}{2T_3}+\frac{W_3}{2}\right)\mu_2 = \Omega_2 u_2 + V_2(\rho_{22}-\rho_{33}) - V_1 u_3,$$

$$\left(\frac{\mathrm{d}}{\mathrm{d}t}+\frac{1}{2T_3}+\frac{W_3}{2}\right)u_3 = -(\Omega_1+\Omega_2)\mu_3 + \mu_2 V_1 - \mu_1 V_2,$$

$$\left(\frac{\mathrm{d}}{\mathrm{d}t}+\frac{1}{2T_3}+\frac{W_3}{2}\right)\mu_3 = (\Omega_1+\Omega_2)u_3 - u_2 V_1 + u_1 V_2,$$

where $V_1 = -d_1E_1/4\pi h$; $V_2 = -d_2E_2/4\pi h$; E_1 and E_2 are the amplitudes of the electric field strength corresponding to the first and second transitions; $\Omega_{1,2}$ are the frequency detunings for the first and second transitions; $u_{1,2}$ and $\mu_{1,2}$ are the in-phase and $\pi/2$-shifted polarisation components, respectively, normalised to the transition dipole moment; u_3 and μ_3 are the real and imaginary parts of the density-matrix element ρ_{13}; $d_{1,2}$ are the transition dipole moments; ω_{32} and ω_{21} are the transition frequencies; $\omega_{1,2}$ are radiation frequencies; A_{ij} are the Einstein coefficients; $T_{2,3}$ are the lifetimes of the second and third levels; and W_3 is the upper-level decay time determined by external processes (photoionisation, superluminescence, and chemical reactions). For copropagating radiation beams, $\Omega_1 = \omega_{21}(1-v/c)-\omega_1$, $\Omega_2 = \omega_{32}(1-v/c)-\omega_2$, while for counterpropagating beams, $\Omega_2 = \omega_{32}(1+v/c)-\omega_2$, where v is the velocity of an atom. It is assumed that the velocity distribution of atoms is described by the Maxwell distribution and the emission line has a Doppler width.

System of equations (1) does not describe the dynamics of the electric field, thereby neglecting the effects related to the deformation of the emission pulse shape and formation of solitons. However, these effects are substantial when atoms not only absorb radiation but also transfer their energy to the radiation field [58]. In experiments on isotope separation, reemission of atoms is undesirable because it reduces the degree of their excitation, and the excitation selectivity decreases due to the dynamic Stark effect. Therefore, we will consider radiation pulses with moderate energies, which, however, are sufficient for exciting a great part of atoms to the upper level.

3.2 Two-photon excitation of lead atoms

Consider the possibility of removing the radioactive ^{210}Pb isotope by the photoionisation method. Lead and lead–tin alloys with low radioactivity are required for the production of microchips with a clock frequency above 500 MHz. Natural lead contains the ^{210}Pb isotope appearing due to decay of ^{238}U. The ^{210}Pb isotope decays to the ^{210}Po isotope, which yields the ^{206}Pb isotope after the alpha decay. Fast alpha particles penetrating into the $p-n$ junction destroy the chip operation. The ^{210}Pb isotope can be removed from lead only by the methods of isotope separation. This problem is virtually ideal for laser isotope separation [55]. The concentration of this isotope in lead is very low, being only $\sim 10^{-13}$ %. In this case, absorption of radiation by ^{210}Pb atoms can be neglected, and there are no problems related to self-focusing of radiation and space–time matching of radiation pulses. This allows the use of quite extended regions of interaction of radiation with matter (several tens of metres).

Fig. 3 shows the energy level diagram for lead atoms, which can be used for photoionisation. The solid arrows denote the possible photoionisation channels, and the dashed arrows indicate spontaneous transitions. The first transition from the ground level to the resonance level is determined virtually unambiguously because transitions to higher levels correspond to too short wavelengths. As for the second transition, two variants were considered, namely, excitation of the $7p\ ^3D_1$ level by a Nd:YAG laser and excitation of the $8p\ ^3D_1$ level by a rhodamine 6G dye laser.

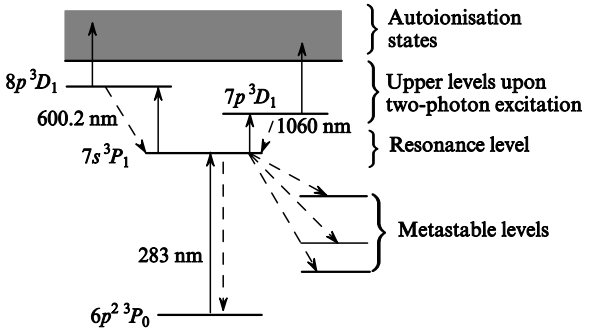

Figure 3. Scheme of transitions in a lead atom.

The Nd:YAG laser was chosen in the first case because its radiation frequency exceeds the transition frequency only by 6 cm^{-1} and can be tuned to an exact resonance by varying the crystal temperature. The choice of the dye laser for photoionisation in the second case was mainly determined by the diagram of autoionisation levels and their lifetimes.

Using the laser unit described above, which provides emission tunable in a broad range, we chose the autoionisation levels with excitation cross sections of about 10^{-15} cm^2. In this case, the photoionisation probability can exceed the probability of the radiative decay of the upper level [11] at moderate powers of ionising radiation.

We performed calculation for determining the conditions that provide the maximum efficiency of the system taking into account restrictions imposed on the radiation parameters.

The choice of radiation parameters for the photoionisation separation of the ^{210}Pb isotope was discussed in paper [55]. The calculations were performed for an ideally collimated atomic beam. The system efficiency was found to depend on the absorption of radiation by atoms of all isotopes, except the ^{210}Pb isotope being separated, whose content in the mixture was extremely small. The minimisation of absorption imposes strict requirements on the detuning value. The latter depends on the pulse energy and duration. For example, the optimal detuning lies in the range from 30 to 60 GHz for the radiation energy density equal to 50 μJ cm^{-2}.

Fig. 4 shows the relative populations of the upper level (n_3) and metastable levels (n_m), and the concentration n_i^+ of

the ^{210}Pb isotope calculated for optimal frequency detunings and delay of the ionising pulse for the $6p^2\,{}^3P_0 \rightarrow 7s\,{}^3P_1 \rightarrow 8p\,{}^3D_2$ transitions. Also, the time profiles of radiation pulses are presented. The calculations were performed for the pulse energy densities at the first and second transitions of 50 μJ cm^{-2}, the pulse FWHM of 15 ns, the average photoionisation probability of the third level of 10^9 s^{-1}, the photoionisation pulse FWHM of 10 ns, and the frequency detuning and deviation of 47 GHz and 30 MHz, respectively. One can see that the degree of ionisation of the ^{210}Pb isotope for these calculations exceeds 0.9. The ionisation degree for other isotopes is close to 0.001.

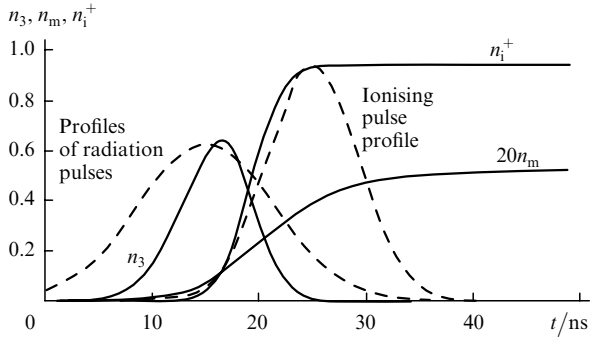

Figure 4. Time dependences of populations of the upper level (n_3) and metastable levels (n_m), and the ion concentration (n_i^+), as well as the profiles of the ionising pulse and radiation pulses.

Demand for lead in which the amount of the ^{210}Pb isotope is reduced 100 – 1000 times compared to its content in natural lead was increased recently in a market of materials for microelectronics. To reduce the content of the ^{210}Pb isotope to such amounts, it is necessary to perform photoionisation of lead several times. A collimated beam of lead atoms passes a distance of 10 cm for the time that is sufficient for photoionisation to occur three times at a pulse repetition rate of 10 kHz. However, the third pulse does not produce already the desired effect because more than 2.5 % of atoms that are not involved in photoionisation are accumulated at metastable levels during one pulse (Fig. 4). Therefore, it is necessary to depopulate the metastable states during the time between the radiation pulses.

When 50 % of radiation at the first transition is used, the ultimate productivity of the laser unit described above is estimated as 1 g s^{-1} (about 2 tones of the isotope product per month at continuous operation). Therefore, the obtaining of low-radioactive lead using this technology [55] becomes a commercial large-scale production.

3.3 Two-photon excitation of boron and silicon atoms

The successful separation of Pb isotopes at a semicommercial scale stimulates the attempts to use this method for separation of other isotopes. Consider the isotope-selective photoionisation of boron and silicon atoms by tunable dye lasers.

The natural content of stable silicon isotopes is 92.2 % of ^{28}Si, 4.7 % of ^{29}Si, and 3.1 % of ^{30}Si. In some technological applications, it is necessary to have very pure silicon isotopes. It is obvious that it is preferable to separate the ^{28}Si isotope, which is contained in the greatest amount in natural silicon. The natural content of stable boron isotopes is 19.9 % of ^{10}B and 80.1 % of ^{11}B. The problem is to separate the ^{10}B isotope from the mixture of two isotopes for the use in a nuclear reactors and to obtain a pure boron isotope for reducing the thickness of the $p-n$ junctions.

It is proposed to use for silicon and boron atoms similar photoionisation schemes involving two-photon excitation of one of the high-lying states through a resonance level. It is important that two-photon excitation is proposed rather than two-step excitation. For silicon, the scheme $3p^2\,{}^3P_2 \rightarrow 4s\,{}^3P_2 \rightarrow 5p\,{}^3D_2$ is suggested and for boron – the scheme $2p\,{}^2P_{1/2} \rightarrow 3s\,{}^2S_{1/2} \rightarrow 4p\,{}^3P_{1/2}$. The wavelengths of these transitions for silicon and boron coincide with an accuracy of 1.5 %. The oscillator strengths of these transitions and the lifetimes of the levels are also close for these atoms, resulting in close optimal energy densities for silicon and boron. Fig. 5 shows energy level diagrams for boron and silicon atoms involved in photoionisation.

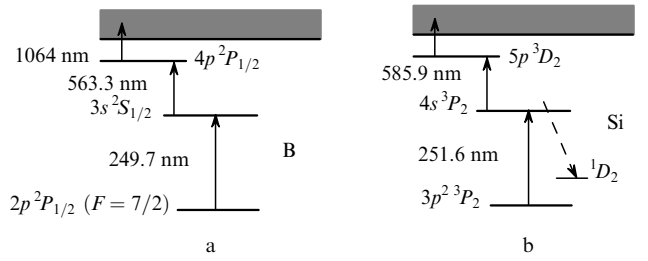

Figure 5. Photoexcitation schemes for boron (a) and silicon (b) atoms.

The choice of the first (the lowest) level is ambiguous. The ground state of boron is split into two sublevels spaced by 15 cm^{-1}. The energy gap between these sublevels is far smaller than the thermal energy of atoms, and we can assume that the levels are populated proportionally to their statistical weights. In addition, each of the sublevels is split into hyperfine-structure sublevels because ^{10}B atoms have nonzero nuclear spin ($I = 3$). Therefore, the levels of the $2p\,{}^2P_{1/2}$ doublet will be split into two hyperfine-structure sublevels, while those of the $2p\,{}^2P_{3/2}$ state into four sublevels. Only one of these six sublevels can be used as a lower level for two-photon excitation. In this paper, we considered only sublevels of the lower level of the $2p\,{}^2P_{1/2}$ doublet with a simpler hyperfine splitting.

The data on the hyperfine structure of the resonance line of the ^{11}B and ^{10}B isotopes are presented in Refs [59, 60]. The selectivity increases with distance of a hyperfine-structure component of the ^{10}B isotope being selected from components of the ^{11}B isotope. In this sense, the component with the total rotation moment $F = 7/2$ has the advantage over the component with $F = 5/2$. The former component is proposed for using as the first lower level for excitation.

The resonance $3s\,{}^2S_{1/2}$ level having a large photoexcitation cross section and the lifetime equal to 4.1 ns is used as the second level [59]. The third level should be long-lived because this reduces spontaneous emission losses and makes the requirements to the power of ionising radiation less stringent. The $4p\,{}^3P_{1/2}$ level having the lifetime equal to 210 ns can be used as the third level [59]; however, the final choice will depend on the ionisation efficiency.

The primary aim of the calculations was to determine radiative parameters corresponding to the maximum

efficiency of the system. It was necessary to find the conditions under which a maximum possible number of ions of the very pure ^{10}B and ^{28}Si isotopes would be produced in an active volume during a single pulse. Note that the radiation energy at the first transition is limited, being ~ 0.1 mJ. The radiation energy at other transitions can be an order of magnitude higher.

We considered a case of a perfectly collimated atomic beam. The lifetimes of the levels and oscillator strengths were taken from Ref. [59]. The radiation pulses at the first and second transition were assumed rectangular, with duration of 10 ns. The characteristic time of ionisation of the third level was chosen equal to 10 ns. The ionising radiation pulse started immediately after the end of the exciting pulse.

The efficiency of two-photon excitation depends on the detuning Δ of the resonance frequency. But especially strongly it depends on the deviation δ (the deviation of a sum of transition frequencies from a sum of laser frequencies). Fig. 6 shows the frequency dependences of the degree of ionisation of boron isotopes. It was assumed that the radiation frequency at the first transition is fixed, whereas the radiation frequency at the second transitions is varied. The oscillations of the frequency characteristic observed both upon one-photon and two-photon excitation are typical for the coherent interaction of radiation with atoms. We can estimate from the logarithmic curve in Fig. 6b the degree of ionisation of the ^{11}B isotope. Upon the frequency shift by 4000 MHz, the degree of ionisation will be approximately four orders of magnitude lower than the maximum degree of ionisation of ^{10}B. The degree of ionisation of silicon isotopes is described by similar dependences.

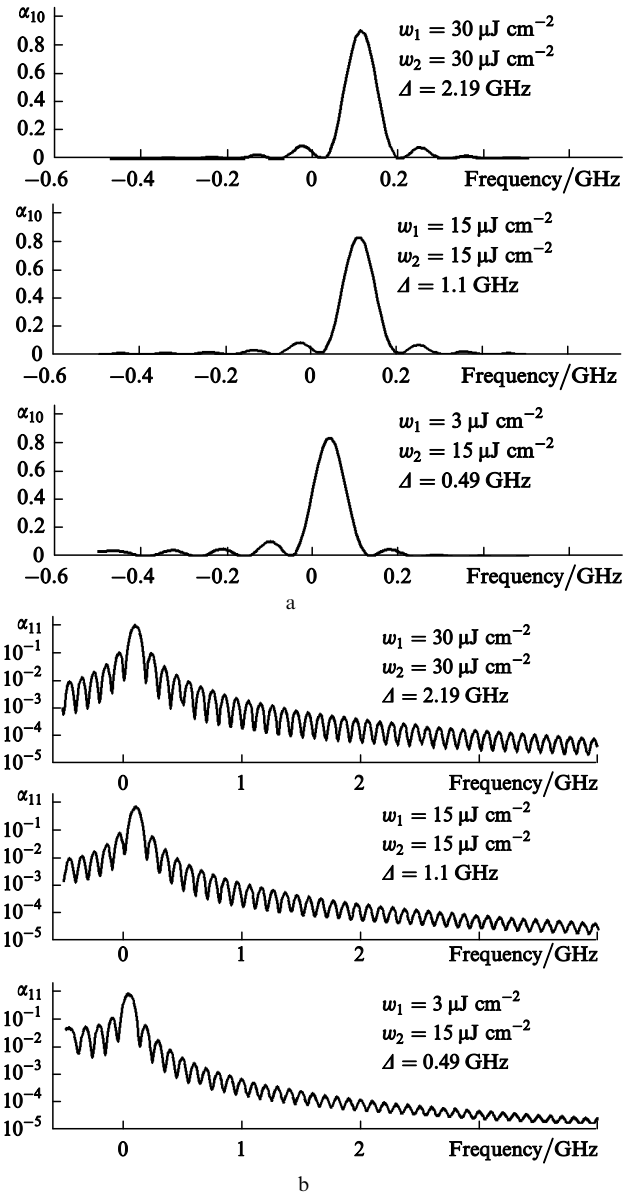

Figure 6. Frequency dependences of the degree of ionisation α_{10} and α_{11} of boron isotopes ^{10}B and ^{11}B, respectively, at the linear (a) and logarithmic (b) scales for different energy densities at the first (w_1) and second (w_2) transitions and different detunings Δ.

For each set of radiation energies, there exists the optimal detuning of the resonance frequency and the optimal deviation. Fig. 7 shows the optimal deviation and the optimal degree of ionisation of boron isotopes as functions of the frequency detuning for the optimal deviation. One can see that the degree of ionisation of ^{10}B atoms has a maximum. The undesirable ionisation of atoms of the ^{11}B isotope drastically decreases in the region of detunings that are smaller than the optimal value; therefore, in the case of boron, the detuning can be chosen equal to its value that are optimal in the degree of ionisation. In this case, as one can see from Fig. 7, the high selectivity is provided.

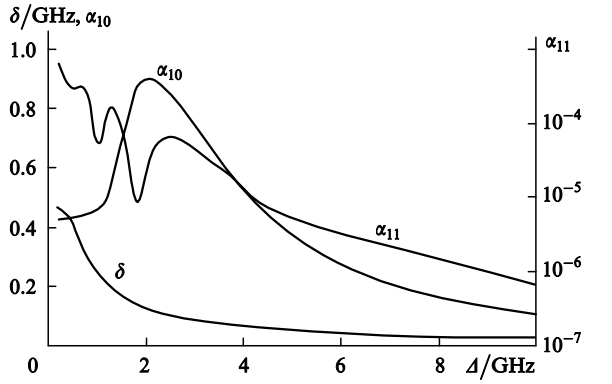

Figure 7. Degrees of ionisation α_{10} and α_{11} of ^{10}B and ^{11}B isotopes, respectively, and the optimal deviation δ as functions of the detuning for the radiation energy density of 30 μJ cm^{-2}.

Similar results were also obtained for silicon atoms. The spectrogram for silicon upon excitation of even isotopes virtually coincides with that for boron. However, because the isotope shift for silicon is approximately an order of magnitude lower, the selectivity of photoionisation of silicon is substantially lower than that of boron. It was assumed that the radiation lines were tuned to the $3p^2\,{}^3P_2 \rightarrow 4s\,{}^3P_2 \rightarrow 5p\,{}^3D_2$ transitions.

Our calculations showed that

(i) the degree of ionisation can achieve 0.9;

(ii) the FWHM of the spectral dependence of the degree of ionisation weakly depends on the pulse energy at the optimal detuning and optimal deviation and is of about 100 MHz; and

(iii) the optimal deviation increases with energy.

The most important result is that the width of the

spectral dependence of the degree of ionisation of about 100 MHz is far smaller than the difference between frequencies of the line being excited and the nearest line of the ^{11}B isotope. This provides the predominant ionisation of the ^{10}B atoms.

The high degree of ionisation of boron and silicon atoms (~ 0.9) can be achieved in a broad energy range by a proper choice of the detuning and deviation. The calculations showed that the pulse energy density of ~ 30 μJ cm^{-2} is quite acceptable. In this case, the detuning is ~ 2 GHz and the deviation is ~ 0.1 GHz. The probability of excitation of the ^{10}B and ^{28}Si atoms is ~ 0.9, of the ^{11}B atoms is 0.00003, and of the ^{30}Si atoms is of about 0.02. This means that the degree of purification of boron can be theoretically extremely high, whereas for silicon it is several orders of magnitude lower.

The productivity of laser isotope separation is determined by the radiation power that can be achieved. As follows from calculations, the degree of ionisation under ideal conditions can be as high as 0.9. Then, approximately one photon is spent per ion at each stage. Knowing the pulse energy, we can estimate the total number of ions in the entire volume. Let us assume for estimate that the power at the first transition, i.e., at 250 nm, is 1 W at a pulse repetition rate of 10 kHz. This corresponds to the production of 1.2×10^{18} ions per second. In the case of a perfect extraction of the ions, the ultimate productivity for boron and silicon is 0.07 and 0.2 g h^{-1}, respectively. However, real values will be smaller. Because of the longitudinal and transverse inhomogeneity of a radiation beam, the radiation intensity will be different in different parts of the active volume, resulting in different degrees of ionisation. In addition, a part of ions will be lost during extraction on the surfaces of the elements of an extractor, which serve to prevent the entry of undesirable isotopes to collectors. All this reduces the ultimate productivity at least by one half. Therefore, the expected real production of these isotopes is no more than 0.03 and 0.1 g h^{-1} for boron and silicon, respectively, for continuous irradiation by 1-W laser beams.

4. Photochemical separation of zinc isotopes using two-photon excitation

4.1 Description of the method

A zinc atom belongs to the elements for which isotope separation in weight amounts by the methods of laser photoionisation is hindered. The main reasons are a poor accommodation of zinc atoms even on cold surfaces and the absence of near-lying autoionisation states. The separation of zinc isotopes by another method was demonstrated in Refs [44, 45]. The method is based on two-photon excitation of Zn to the $6s\,^3S_1$ state upon absorption of two counterpropagating photons with wavelengths $\lambda_1 = 0.307$ μm and $\lambda_2 = 0.303$ μm (Fig. 8). The close energies of these photons involved in the two-photon process reduces the Doppler broadening down to 20 MHz, which is substantially lower than isotope shifts. The $6s\,^3S_1$ state is then transformed to the $4p\,^3P^0$ state after a chain of spontaneous and stimulated transitions occurring both through the intermediate levels $5p\,^3P^0_{0,1,2}$ and $5s\,^3S_1$ and directly.

Because the intersystem crossing between the singlet and triplet levels of the Zn atom are very weak, all the atoms

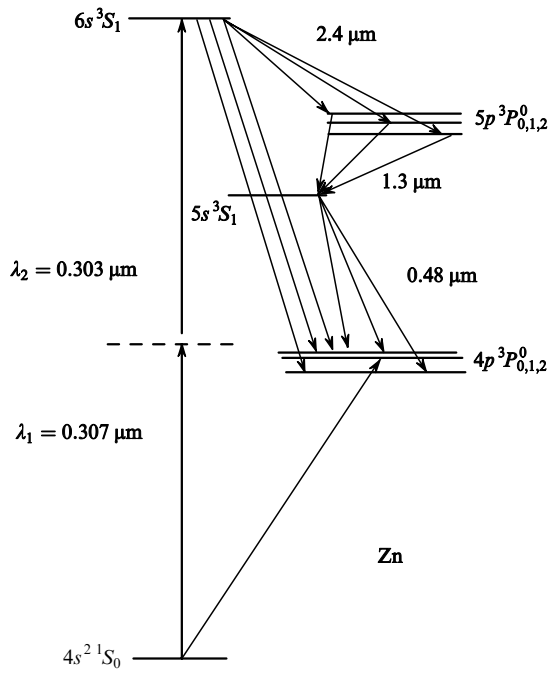

Figure 8. Scheme of transitions in a zinc atom.

populate the $4p\,^3P^0$ state after two-photon excitation due to fast processes occurring faster than for 30 ns. To prevent isotope-non-selective direct excitation of Zn atoms during one-photon pumping at the first intercombination transition, the laser frequency was detuned from the exact resonance by four-five Doppler half-widths.

The desired isotope was separated in the photochemical reaction

$$\mathrm{Zn}^*(4p\,^3P_{0,1,2}) + \mathrm{CO_2} \rightarrow \mathrm{ZnO} + \mathrm{CO} + Q,$$

whose rate constant was $k = 2.5 \times 10^{-10}$ cm^3 s^{-1}, which is four-five orders of magnitude higher than the reaction rate for an unexcited atom at working temperatures; $Q = 1.3$ eV. This provides a high selectivity of the process. For a pressure of CO_2 equal to 0.1 Torr, the reaction rate is an order of magnitude higher than the probability (10^5 s^{-1}) of spontaneous decay of the $6p\,^3P^0_j$ state, while the quantum efficiency exceeds 50 %. The product of this reaction, as some other reactions, is the stable compound ZnO, which is deposited on a collector. The rest of reagents are evacuated from the region of isotope separation.

The isotopes were separated in the CO_2 flow with Zn vapour at a relatively high pressure of CO_2 (~ 1 Torr). Because the concentration of Zn atoms was low ($\sim 10^{13}$ cm^{-3}), a high flow rate of Zn through a working cell of a separation unit should be used to enhance the productivity. The number N_a of the reacted atoms is equal to the number of absorbed photons: $N_a = P_{ab}/h\nu$, where P_{ab} is the absorbed power and $h\nu$ is the energy of a resonance photon. For $P_{ab} = 2$ W, the number of reacted atoms is $N_a = 3.2 \times 10^{18}$ atm s^{-1}, which corresponds to the flow rate equal to 320 L s^{-1}. The pressure of CO_2 is approximately three orders of magnitude greater, which causes difficulties upon circulation of CO_2 and Zn vapour in a common flow. For this reason, the working mixture was pumped in the following way: CO_2 was pumped along the

laser beam at a rate of ~ 2 L s^{-1}, while the Zn vapour was pumped perpendicular to the laser beam, from an evaporator to a cold wall. A collector for collecting the isotopically enriched zinc oxide was placed in the pumping region.

4.2 Polarisation of radiation

The photoexcitation scheme $4s\,^1S_0 \rightarrow 4p\,^3P_1 \rightarrow 6s\,^3S_1$ proposed above does not work when laser beams with parallel linear polarisations are used. Such a transition is forbidden by selection rules. For linearly polarised light, the magnetic quantum numbers are $M = M'$, which permits the separation of individual photoexcitation channels. However, the transition is forbidden if $M = M' = 0$ and $J = J'$ (where J is the rotational quantum number). The first transition in this scheme separates an individual channel with $M = 0$, i.e., the relation $M = M' = 0$ should be fulfilled for all transitions, but $J = J'$ for the second transition, and, hence, the transition is forbidden. In such cases, the prohibition can be removed by using circularly polarised light [57], which, however, involves practical problems because it is difficult to control the degree of ellipticity of radiation and the quality of $\lambda/4$ plates. The measurements of absorption of light in an active medium strongly depend on the orientation of these plates.

The theoretical analysis showed that two linear mutually perpendicular polarisations can be used instead of circular polarisations. Because of a limited volume of the paper, we will not present here a detailed theoretical analysis but give only quantitative explanation.

Let us assume that polarisation planes of radiation at the first and second transitions are mutually perpendicular. Consider two coordinate systems in which quantisation axes z are directed along polarisation of radiation at these transitions. Upon the replacement of one coordinate system by another, the state with $M = 0$ at the second level will transform to a combined state with $M = -1$ and $M = 1$ in a new coordinate system according to the transformation rules for ψ functions [61]. Linearly polarised radiation at the second transition from these states excites levels with the same values of M at the third level. Therefore, the third level can be excited by using crossed linear polarisations.

To avoid the consideration of all the states with different M in equations for the density matrix, we can use the following formal procedure. It is known [61] that instead of a set of the eigenfunctions of degenerate states, an equivalent orthonormalised basis of linear combinations of these functions can be used. We will use in the quantisation along the radiation propagation a set of eigenfunctions at which radiation polarised along the x axis excites at the second level only one component of the basis. As a such set, the system of functions

$$\varphi_{-1} = \frac{\mathrm{i}}{2}(\psi_1 - \psi_{-1}) + \frac{1}{\sqrt{2}}\psi_0, \quad \varphi_0 = \frac{\mathrm{i}}{\sqrt{2}}(\psi_1 + \psi_{-1}),$$
$$\varphi_1 = \frac{\mathrm{i}}{2}(\psi_1 - \psi_{-1}) - \frac{1}{\sqrt{2}}\psi_0, \tag{2}$$

can be used, where the subscripts denote the values of the magnetic quantum number. The set of functions (2) corresponds to the orthonormalised basis. While in the old basis, two components ψ_{-1} and ψ_1 were excited, now only one component φ_0 is excited. Indeed, the dipole moment $\langle\varphi_i|d_x|\psi_g\rangle$ (where ψ_g is the ψ function of the ground state) is nonzero only for the transition to the φ_0 state:

$$\langle\varphi_0|d_x|\psi_g\rangle = \left\langle \frac{\mathrm{i}}{\sqrt{2}}(\psi_1 + \psi_{-1}) \middle| \frac{(d_{-1} + d_{+1})}{2} \middle| \psi_g \right\rangle$$
$$= \left\langle \frac{\mathrm{i}}{\sqrt{2}}\psi_1 \middle| \frac{d_{-1}}{2} \middle| \psi_g \right\rangle + \left\langle \frac{\mathrm{i}}{\sqrt{2}}\psi_{-1} \middle| \frac{d_{+1}}{2} \middle| \psi_g \right\rangle$$
$$= \frac{\mathrm{i}}{2\sqrt{2}}(d_{-1} + d_{+1}) = \frac{\mathrm{i}}{\sqrt{2}}d_{-1}, \tag{3}$$

where d_{-1} and d_{+1} are the dipole moments for left-hand and right-hand circular polarisations. The dipole moments for other states in (2) are zero.

Similarly, upon excitation of the third level by y-polarised radiation, only the $\varphi_0 \rightarrow \psi_0$ transition has a nonzero dipole moment

$$\langle\psi_0|d_y|\varphi_0\rangle = -\frac{1}{\sqrt{2}}d_{-1}, \tag{4}$$

where ψ_0 is the state of the third level with $M = 0$. For the corresponding transitions (the subscripts are omitted), we have

$$d_x = \frac{1}{\sqrt{3}}d, \quad d_y = \frac{1}{\sqrt{3}}d. \tag{5}$$

The dipole moment d can be expressed in terms of the oscillator strength f (in absorption) [62]:

$$d^2 = \left(\frac{3he^2}{2m_e}\right)\frac{f(2J+1)}{\nu}. \tag{6}$$

Therefore, two-photon absorption can be calculated in the scheme $1\psi_0 \rightarrow 2\varphi_0 \rightarrow 3\psi_0$ by neglecting additional levels with different magnetic numbers. The initial system of equations for the density-matrix elements remains the same. One can easily show that matrix elements of perturbations in the case of using circular polarisations at the same radiation intensity are exactly equal to the matrix elements when linear polarisations are used. Therefore, the use of linear polarisations, which compares well in its ultimate efficiency with the use of circular polarisations, has an advantage of simplicity of technical implementation.

4.3 Mathematical model of cascade superluminescence

Experiments on laser isotope separation showed that upon two-photon excitation of zinc atoms, absorption of light nonlinearly depends on the concentration of the atoms. This is explained by the development of cascade superluminescence. Several lines were observed at 2.4, 1.3, and 0.45 μm. The power of superluminescence measured at 1.3 μm was ~ 100 mW. The presence of superluminescence causes the undesirable broadening of the absorption line at the pump wavelength. As a result, the efficiency of two-photon excitation is reduced by several times. For this reason, comparatively low concentrations of atoms should be used.

Two-photon excitation is accompanied by the energy dissipation due to spontaneous and stimulated transitions. Fig. 8 shows twelve possible transitions. Some transitions may result in the population inversion and the development

of superradiance, whereas the others do not produce inversion. Superluminescence was observed at three transitions $6s\,^3S_1 \rightarrow 4p\,^3P_{0,1,2}$.

The power of spectral lines and population of the levels can be calculated using an incoherent model. Because all atoms in the Doppler profile are excited in the two-photon process in counterpropagating laser beams approximately identically, one can expect that the width of superradiance lines will be of the order of the Doppler width. The coherence time of radiation cannot be longer than the inverse width of the spectrum. In addition, the coherence time of superluminescence cannot exceed the time of radiation passage in the active region. Therefore, radiative transitions can be characterised by transition cross sections, which occurs in the incoherent case.

The population kinetics can be analysed in the saturated power approximation [63] assuming that $N_2/g_2 = N_1/g_1$, where the subscripts 2 and 1 refer to the upper and lower levels, respectively. However, in our case, it is desirable to use a less strict condition

$$\frac{\mathrm{d}}{\mathrm{d}t}\left(\frac{N_2}{g_2} - \frac{N_1}{g_1}\right) = 0, \tag{7}$$

i.e., the level populations per unit of the statistical weight can differ by a constant. Indeed, the saturated power approximation follows from the equation for the photon density

$$\frac{\mathrm{d}}{\mathrm{d}t} n_\mathrm{p} = P - \frac{n_\mathrm{p}}{\tau}, \tag{8}$$

$$P = c\sigma n_\mathrm{p} g_2 \left(\frac{N_2}{g_2} - \frac{N_1}{g_1}\right), \tag{9}$$

$$\sigma = \frac{1}{4}\pi \left(\frac{\ln 2}{\pi}\right)^{0.5} \frac{A\lambda^2}{v_\mathrm{d}}, \tag{10}$$

where P is the rate of photon arrival due to stimulated transitions; τ is the photon lifetime in the active medium; σ is the stimulated transition cross section; A is the spontaneous emission probability; and v_d is the Doppler width. The derivative in (8) is estimated as $n_\mathrm{p}/\tau_\mathrm{pul}$, where τ_pul is the pulse duration, and it can be neglected compared to n_p/τ in the right-hand of (8) because $\tau_\mathrm{pul} \gg \tau$ (τ does not exceed the time of radiation passage through the active region). Then,

$$P = \frac{n_\mathrm{p}}{t}, \tag{11}$$

and we obtain the threshold condition

$$\frac{N_2}{g_2} - \frac{N_1}{g_1} = \frac{1}{\tau} c\sigma g_2. \tag{12}$$

The equations for populations can be written in the form

$$\frac{\mathrm{d}}{\mathrm{d}t} N_2 = G_2 - P, \tag{13}$$

$$\frac{\mathrm{d}}{\mathrm{d}t} N_1 = G_1 + P, \tag{14}$$

where $G_{1,2}$ are the rates of change in the level populations caused by all process except stimulated processes. Taking into account (12), we obtain from (13) and (14)

$$P = \left(\frac{G_2}{g_2} - \frac{G_1}{g_1}\right) \frac{g_1 g_2}{g_1 + g_2}. \tag{15}$$

The threshold condition (12) imposes restrictions on some transitions. Let us call two combinations of transitions starting and terminating on the same levels the conjugated cascade transitions. It can be readily shown that superluminescence will develop only in the conjugated transition for which $\sum (g_1 f/v_\mathrm{d})^{-1}$ achieves the minimum value (the summation is performed over all, transition in the cascade). This condition prohibits the development of superluminescence at the $6s\,^3S_1 \rightarrow 4p\,^3P_{0,1,2}$ transitions and transforms the graph of possible transitions to a 'tree-like graph', which substantially simplifies the calculation of radiation powers at different transitions. The successive use of the above procedure leads to a system of differential equations for level populations and a system of linear algebraic equations for the radiation power. The matrix of the system can be inverted once, and the radiation power can be automatically calculated for each value of level populations.

When the kinetics of level populations in the cascade (except the upper level) is determined only by stimulated emission, the calculation becomes very simple. We can show that, if there exists an unbranched cascade of transitions, then the power at any transition can be found from the expression

$$P_{i+1} = \frac{P_i g_\Sigma}{g_\Sigma + g_{i+1}}, \tag{16}$$

where P_i is the rate of excitation due to stimulated transitions at the ith transition; g_i is the statistical weight of the upper level of the transition; and g_Σ is the total statistical weight of all levels downward the cascade, including the lower level of the transition. The excitation rate of the upper level is determined by the two-photon excitation rate. The recurrent expression (16) allows one to find the powers at all other transitions.

In another case, when radiation is emitted from one upper level to several lower levels, the total excitation rate of lower levels due to stimulated transitions can be calculated from the expression

$$P_\Sigma = \frac{G g_\Sigma}{g_\Sigma + g_2}. \tag{17}$$

which is similar to (16). Here, g_2 is the statistical weight of the upper level. The photon density is distributed proportionally to the statistical weights of lower levels.

The cases considered above show that the rate of population caused by stimulated transitions can be found by calculating the statistical weights of all the levels downward the transition graph tree and using expression (16) or (17). Because we are interested in the total rate of stimulated transitions from the third level in the two-photon process, it is sufficient to calculate the excitation rate due to stimulated emission at three transitions from the upper level and to use expression (17). In our case, the statistical weights are $g_\Sigma = 21$ and $g_2 = 3$.

4.4 Results of calculations

We interpreted our experimental results and estimated the efficiency of the method by performing the numerical simulation of the dynamics of level populations. Because the radiative lifetimes of the working levels proved to be longer than the duration of laser pulses (5–15 ns), it was necessary to describe processes in the approximation of coherent interaction of radiation with matter, taking into account the Doppler velocity distribution of atoms.

According to our calculations, the use of counter-propagating beams can provide efficient excitation (0.7) of zinc atoms to the long-lived $4p\,^3P^0_{0,1,2}$ states. These states are populated due to radiative transitions from the upper level. As shown above, the optimal deviation exists for each detuning. The atoms moving at different velocities have substantially different detunings. A change in the deviation depends on the difference between the wavelengths at the first and second transitions. If the deviation remains close to its optimal value for different atoms of the Doppler contour, the efficient excitation of all the atoms will be provided.

The relation $\mathrm{d}\delta_{\mathrm{opt}}(\Delta + v - v_0)/\mathrm{d}v \sim (\lambda_2 - \lambda_1)/\lambda$ can serve as a criterion for the efficiency of using counterpropagating beams. Here, v_0 is the central emission frequency of the Doppler contour; Δ is the frequency detuning for an atom at rest (it is assumed that $|\lambda_2 - \lambda_1| \ll \lambda$ and the width of the Doppler contour does not exceed Δ). In the case of a zinc atom, this relation is approximately fulfilled in the region of radiation energies used in experiments. Because the optimum deviation decreases with increasing detuning (Fig. 7), it is desirable that the difference of the wavelengths at the first and second transitions would be negative, which is the case for zinc atoms.

Fig. 9 shows the dependences of the degree of excitation of the Zn isotope on the radiation frequency shift at the second transition calculated for different concentrations of the isotope. One can see that the linewidth increases with increasing concentration of zinc atoms. This is explained by the development of superluminescence from the upper level to several low-lying levels, which results in the broadening of the line. Absorption increases with increasing concentration

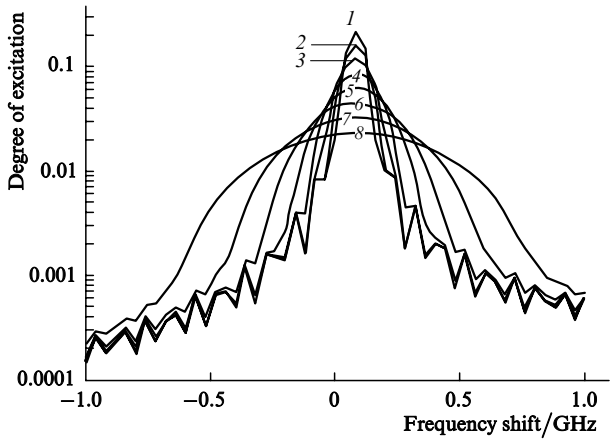

Figure 9. Frequency dependence of the degree of excitation of Zn for the concentrations of atoms of an isotope being separated equal to 2×10^{12} (*1*), 4×10^{12} (*2*), 8×10^{12} (*3*), 16×10^{12} (*4*), 32×10^{12} (*5*), 64×10^{12} (*6*), 128×10^{12} (*7*), and 256×10^{12} cm^{-3} (*8*). The pulse energy is 250 μJ cm^{-2} and the detuning is 7 GHz.

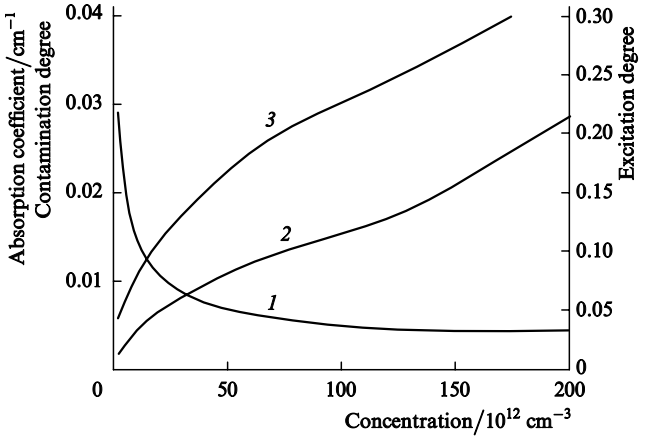

Figure 10. Dependences of the degree of excitation (*1*), the absorption coefficient (*2*) and the contamination degree (*3*) on the concentration of atoms of a zinc isotope for the pulse energy of 250 μJ cm^{-2} and the detuning of 7 GHz.

of zinc atoms, resulting in the increase in the population of the upper level and the enhancement of superluminescence accompanied by the line broadening. One can see from Fig. 9 that superluminescence does not appear at the line wings, and therefore it cannot affect the efficiency of excitation of neighbouring isotopes (the transition frequency for a nearest isotope is shifted by 660 MHz). However, the separation selectivity decreases because the degree of excitation at the line centre decreases.

Fig. 10 shows the calculated dependences of the degree of excitation of zinc isotopes, the absorption coefficient, and the degree of excitation of the levels of unnecessary isotopes (the contamination degree) on the concentration of the isotope being separated. One can see that absorption of radiation and the degree of excitation of the levels of unnecessary isotopes increase nonlinearly with the concentration of atoms. These dependences are in satisfactory agreement with the experimental results. Our calculations showed that the degree of excitation of unnecessary Zn isotopes equal to 1 % is achieved when the absorption coefficient does not exceed 0.004 cm^{-1}. The experimental measurements of the absorption coefficient yield close values.

4.5 Experimental results

Fig. 11 shows luminescence spectra as functions of the frequency detuning $\delta\nu_2$ of the second transition, which demonstrate separation of Zn isotopes. For low concentration of Zn and the moderate power of lasers, a completely resolved isotopic structure is obtained (Fig. 11a). The ultimate width of the spectrum of an individual isotope is 70 MHz. For high concentration of atoms (Fig. 11b) or high power density (Fig. 11c), the lines of two-photon resonance are strongly broadened and can overlap completely (Fig. 11d).

Our experimental data showed, in accordance with calculations, that the width of the absorption line increased with increasing concentration of isotope atoms or radiation intensity. This effect can be explained by an increase in the radiation absorption and, hence, in the superradiance power, resulting in an increase in the frequency of stimulated transitions. This leads to an increase in the absorption linewidth and a decrease in the selectivity of isotope

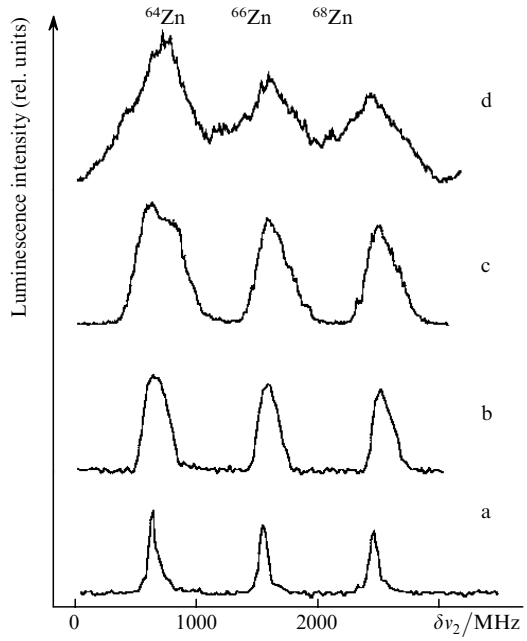

Figure 11. Luminescence spectra at 1.3 μm as functions of $\delta\nu_2$ ($\delta\nu_1 = 5$ GHz) for E_1, $E_2 = 150$ μJ cm^{-2}, $n = 1.6 \times 10^{13}$ cm^{-3} (a), E_1, $E_2 = 150$ μJ cm^{-2}, $n = 2.4 \times 10^{14}$ cm^{-3} (b), E_1, $E_2 = 400$ μJ cm^{-2}, $n = 1.6 \times 10^{13}$ cm^{-3} (c), and E_1, $E_2 = 550$ μJ cm^{-2} and $n = 1.6 \times 10^{13}$ cm^{-3} (d).

separation. For a given selectivity of isotope separation, this effect restricts from above the laser power and the concentration of an isotope being separated.

Because the requirements to the efficiency and selectivity contradict to each other, an optimal relation between the specific productivity, efficiency, and selectivity of isotope separation should be found in each specific case. For example, when the selectivity is 50 – 100, the radiation energy density E_1 and E_2 should not exceed 350 μJ cm^{-2} for the detuning $\delta\nu_1 = 9$ GHz, while the concentration of zinc atoms should be no more than 2×10^{13} cm^{-3}. Under these conditions, the absorption coefficient for the ^{66}Zn isotope is $k_\nu \sim (3 - 4) \times 10^{-3}$ cm^{-1}, which allows the efficient use of the pump radiation (up to 50 %) in cells of length 150 – 200 cm. The productivity of the unit in this case amounts to 0.6 g h^{-1}, and commercial isotope products of purity 98 % was obtained.

5. Photochemical isotope separation using one-photon excitation of long-lived levels

5.1 Experimental method

The method of two-photon excitation is inefficient for some atoms whose isotopic structure is masked by the Doppler broadening. This is explained by the fact that this method requires the use of two high-power tunable UV lasers, which complicates a laser setup for isotope separation and makes it more expensive. In addition, it is impossible sometimes to find efficient excitation schemes.

In papers [52, 53], another method of isotope separation was demonstrated for zinc and rubidium atoms, which can be used for many elements. The method is based on one-photon selective excitation of long-lived atomic states. Atoms in long-lived excited states can take part in efficient chemical reactions with some molecules, whereas the reaction rate in the ground state is low. The method uses radiation at one wavelength, it does not require the collimation of atomic beams and does not need an electric extraction. It uses the property of a Doppler profile consisting in the fact that the excitation selectivity increases with increasing the frequency detuning simultaneously from the frequencies of lines of all isotopes.

It is interesting to note that, on the contrary, for a Lorentzian profile the selectivity asymptotically decreases. One excitation pulse with a narrow spectrum excites a small fraction of atoms. Nevertheless, the isotope whose absorption line is the most close to the laser line can be 'burnt out' completely for several thousands of pulses. In this case, the conditions can be provided under which the concentrations of atoms of other isotopes decrease only weakly.

To provide multiple action of radiation on atoms, the transverse or longitudinal circulation of an atomic flow with a low rate is used. In many cases, simultaneously several isotopes can be 'burnt out' during one passage of an atomic flow through the active region, retaining the required isotopes. Excitation into separate hyperfine-structure components of odd isotopes results in their efficient mixing due to multiple collisions. This allows one to remove one isotope completely by exciting only into one component.

In the experiment in Fig. 12, the separation chamber represented a quartz or glass tube of length 60 cm and diameter 3 cm, which was heated with an external oven. A gas flow consisting of atoms under study with argon and reagent-gas molecules circulated in the chamber at a velocity of 0.5 L s^{-1}. The argon pressure was 1 – 2 Torr and the concentration of reagent-gas molecules was 10^{16} cm^{-3}. Under these experimental conditions, the drift time of atoms through the interaction region was of the order of 1 s.

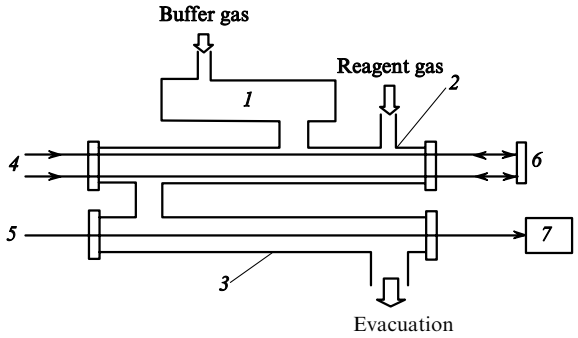

Figure 12. Scheme of the experimental setup for separation of zinc and rubidium isotopes by the one-photon method: (*1*) reservoir with Zn (Rb); (*2*) separation chamber; (*3*) collector chamber; (*4*) laser radiation; (*5*) probe laser radiation; (*6*) mirror; (*7*) photodetector.

The atoms of an isotope under study entered the separation chamber from a reservoir, which was heated with a special oven up to the temperature that provided the required concentration of atoms. The laser radiation propagated along the gas flow, providing 'burning out' of excited atoms due to a chemical reaction. The molecules being formed precipitated on the walls of the separation chamber, while vapours of the elements were condensed on the walls of the collector chamber to which the gas flow entered. The required isotopes were produced using the two-dimensional circulation system described above.

5.2 Mathematical model

We will assume below that the interaction of radiation with atoms is incoherent. This means that at least one of the three conditions is fulfilled:

(i) The radiation linewidth is far greater than the inverse pulse duration;

(ii) the degree of excitation of atoms is far less than unity;

(iii) the transverse relaxation time is much shorter than the pulse duration.

In addition, we will consider excitation by 10 – 100-ns pulses with pulse repetition rates of 1 – 20 kHz. Such a regime is typical for pumping dye lasers by a copper vapour laser. The second harmonic of a Nd : YAG laser can be also used for pumping. Because we consider excitation of levels with lifetimes in the microsecond range, their spontaneous decay during the laser pulse can be neglected.

The initial equations during the laser pulse can be reduced to the known equations of radiation transfer and to kinetic equations. In somewhat modified form for nonpolarised radiation, they can be written as

$$\frac{\partial I}{\partial t} + c\frac{\partial I}{\partial z} = -cI\sum_i \sigma_i m_i, \tag{18}$$

$$\frac{\partial m_i}{\partial t} = \beta_i \sigma_i I m_i, \tag{19}$$

$$n_i = \frac{m_i + (\beta_i - 1)n_{0i}}{\beta_i}, \tag{20}$$

$$\beta_i = 1 + \frac{g_{1i}}{g_{2i}}, \tag{21}$$

where I is the radiation intensity; m_i is the quantity related to the ground-state population n_i varying during the pulse and to the constant total concentration n_{0i} of the ith isotope by expressions (20) and (21); and g_{1i} and g_{2i} are the statistical weights of the lower and upper levels, respectively.

The quantity σ_i is defined by the known expression

$$\sigma_i = \frac{1}{8\pi}\frac{\lambda^2}{\tau_{si}}, \tag{22}$$

where τ_{si} is the radiative lifetime of the level for the transition under study and λ is the wavelength. The equations are written for some fixed frequency.

The line profile $I(v)$ represents a convolution of the emission line profile and of the corresponding Lorentzian profile in the case of the collision or field broadening of the absorption line.

The integration of differential equations (18) and (19) yields the system of equations

$$\frac{\mathrm{d}W(z)}{\mathrm{d}z} = \sum_i \frac{1}{\beta_i}[1 - \exp(1 - \sigma_i\beta_i W)]n_{0i}\,, \tag{23}$$

$$n_i(z) = n_{0i}(z)\exp[-\beta_i\sigma_i W(z)], \tag{24}$$

where $W(z)$ is the number of photons in a pulse per unit frequency interval, per unit cross section propagated through a cross section with the coordinate z. It is important that the state of the medium after pulse propagation depends only on the pulse energy rather than on its shape.

Note that β_i and σ_i can be somewhat different only for the hyperfine-structure components. In many cases, this difference is unsubstantial for isotope separation. For example, the main isotopes of zinc do not have a hyperfine structure, while the hyperfine splitting in boron is approximately an order of magnitude smaller than the isotope shift. In addition, the excitation selectivity depends first of all on the detuning from the transition frequency and only very weakly on the difference in the absorption cross sections and the ratio of statistical weights.

Assuming that the above quantities are the same for all isotopes, we can obtain an exact analytic solution of equations (18) and (19). By using the solution for m obtained in Ref. [64] and expression (2), we can obtain the expression for the change in the concentration of atoms in the ground state for some fixed isotope (the subscript i is omitted for simplicity)

$$\Delta n = -n_0\left[\frac{1 - f(z)}{\beta}\right], \tag{25}$$

where

$$f(z) = \frac{\exp[\sigma p(z)]}{\exp[\sigma p(z)] + \exp(\beta\sigma W_0) - 1}; \tag{26}$$

$$p(z) = \sum_i \int_0^z n_{0i}(z)\mathrm{d}z; \tag{27}$$

W_0 is the number of photons in a pulse per unit frequency interval, per unit cross section. The summation in (27) is performed over all isotopes.

Therefore, there is no need to solve the transfer equations and kinetic equations during the pulse. The period between pulses is described by a system of usual kinetic equations. These equations should take into account chemical reactions, spontaneous decay of the levels, and exchange reactions. However, due to the high selectivity, only a very small fraction of atoms of each isotope is excited during the laser pulse. Therefore, it is necessary to perform calculations for several thousands pulses, by determining the variations in the level populations at different points and at different radiation frequencies. All this requires time-consuming computer calculations of numerous integral characteristics.

However, the situation can be substantially simplified under certain conditions. For this purpose, we will use the frequency-integrated ground-state concentrations of an isotope. The frequency-integrated change ΔN in the ground-state population can be conveniently written in the form

$$\Delta N = -\alpha N_0\left[\frac{1 - f_0(z)}{\beta}\right], \tag{28}$$

where f_0 can be calculated from (26) at the central frequency of the emission contour. The coefficient α in (28) is a fraction of atoms which absorb the laser line:

$$\alpha = \int_0^\infty \frac{f(v)n_0(v)\mathrm{d}v}{f_0 N_0}. \tag{29}$$

Let us also assume that the level populations depend substantially only on a chemical reaction with atoms in excited states with the characteristic time τ_{ch} and spontaneous emission with the lifetime τ_s. In addition, we assume that these times are much shorter than the time interval τ_f between laser pulses, i.e., τ_{ch}, $\tau_s \ll \tau_f$. Then, the concentration of atoms will change to the beginning of the next pulse by the value that is somewhat smaller than that predicted by expression (28) because a fraction of excited atoms will undergo the radiative decay to the ground state. In this case,

$$\Delta N = -\alpha N_0 \left[\frac{1-f_0(z)}{\beta}\right] \frac{\tau_s}{\tau_{ch}+\tau_s}. \tag{30}$$

Because, as noted above, only a very small fraction of atoms is excited during the laser pulse, the evolution of N at the time scale substantially exceeding the interval τ_f between pulses can be written in the differential form

$$\frac{\partial N}{\partial t} + V\frac{\partial N}{\partial z} = -\frac{\alpha N}{\tau_f}\left[\frac{1-f_0(z)}{\beta}\right]\frac{\tau_s}{\tau_{ch}+\tau_s}, \tag{31}$$

where V is the gas flow velocity. Equation (31) takes into account the transfer of atoms by a longitudinal gas flow. A homogeneous flat transverse flow will be described by the same equation, only the coordinate z in the left-hand side of (31) should be replaced by the coordinate x or y. In this case, a two-dimensional distribution of the concentration of atoms will take place. Because the stationary concentration is established for the time approximately equal to the time of the gas passage through the active medium and much shorter than the technological time of the process, the time derivative in (31) can be neglected. Equation (31) is valid for the concentration of atoms of any isotope. The separation selectivity is provided by the different values of α for different isotopes.

By passing to the dimensionless coordinate $z' = z/L$ in equation (31) and the dimensionless concentration of atoms $\eta = N(z)/N(0)$, where L is the active region length, we can see that the solution of the equation depends on the parameters $LN(0)$ and V/L (only on V in the case of a transverse flow). This means that the concentration of atoms in such regimes can be varied by changing L in a proper way (and V in the case of a longitudinal flow).

By assuming that α is constant in (31), we can obtain the relation

$$\eta_i = \eta_j^{\alpha_i/\alpha_j} \tag{32}$$

between the reduced concentrations of the ith and jth isotopes at any point of the active region in the steady-state regime. Let us assume, for example, that the ratio of the numbers of atoms excited per pulse for two isotopes is $\alpha_i/\alpha_j = 10$. Assume also that the concentration of atoms of the jth isotope decreased by half at the end of the flow, whereas the concentration of atoms of the ith isotope decreased by a factor of 2^{10}. Therefore, the ith isotope is virtually completely burnt out, whereas the loss of the jth isotope is quite acceptable.

Equation (31) neglects the reactions of resonance energy transfer between the atoms and isotopic chemical exchange. These reactions restrict from above the admissible concentration of atoms, obviously deteriorating the excitation selectivity. The effect of these reactions can be eliminated by reducing the atomic concentration. To retain simultaneously a sufficiently high absorption, it is necessary to increase the length of the active region. The cross section for the dipole-dipole energy transfer is inversely proportional to the upper-level lifetime [65]. Because we are interested in long-lived states (with lifetimes of several microseconds or longer), we can hope that the cross section will be several orders of magnitude lower than that for typical energy transfer from a resonance level ($10^{-12} - 10^{-13}$ cm^2) [65]. Assuming that the cross section for energy transfer from long-lived states is $\sim 10^{-14}$ cm^2 and taking into account that the characteristic time of energy transfer should be no shorter than the excited-state lifetime, we obtain the upper bound for the atomic concentration $\sim 10^{14}$ cm^{-3}. This value is three order of magnitude greater than the ultimate concentration of atoms acceptable in the AVLIS technology.

Therefore, we obtained the system of integro–differential equations, which allows one to avoid solving the system of equations from pulse to pulse.

5.3 Calculations on separation of zinc isotopes

The calculations were performed both for the transverse and longitudinal gas flows and gave similar results. They demonstrated the efficient burning out of isotopes whose absorption lines were most close to the laser line. Thus, to reduce the concentration of the ^{68}Zn isotope by a factor of ten using 1-W radiation, 2.5 photons are required per atom. In this case, the concentration of the ^{66}Zn isotope decreased by 30 % and that of the ^{64}Zn isotope by 5 %.

The method is especially efficient for obtaining isotope whose line is extreme in the emission spectrum. For example, in the numerical experiment with a radiation power of 2 W, the ^{64}Zn isotope contaminated by 1 % of other isotopes was obtained. In this case, the energy 'cost' of the isotope production was 9 photons per atom. However, if the emission line of the isotope is located in the middle of the spectrum, the energy cost increases because several separation cycles are required. According to our calculations, in this case 50 photons per atom are already required for obtaining the ^{66}Zn isotope with a contamination degree of 1 %.

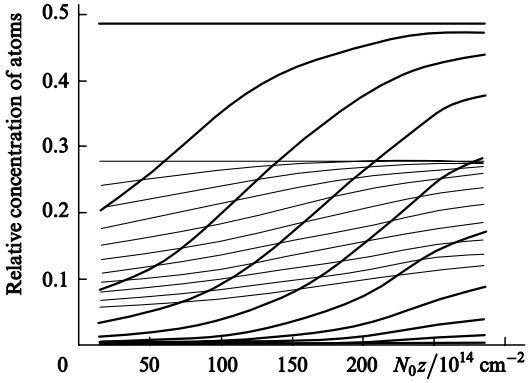

Figure 13. Spatial distribution of ^{64}Zn (thick curves) and ^{66}Zn (thin curves) isotopes. The curves are drawn through each fifty pulses. The numbers of pulses corresponding to the curves increase, beginning from the horizontal straight line, with decreasing concentration of isotope atoms. Radiation is directed along the increasing coordinate.

Transverse gas circulation. The position of atoms along the gas flow can be conveniently characterised by the number of radiation pulses acting on them. Fig. 13 shows the typical dependences of the concentration of atoms of isotopes on the coordinate z along the chamber axis (more precisely, on $N_0 z$, where N_0 is the total concentration of atoms) and their variation from pulse to pulse (the gas flow is directed perpendicular to the z axis). One can see the deformation of the coordinate profile of the concentration of the ^{64}Zn and ^{66}Zn isotopes after each 50 pulses.

The distribution of atoms at the flow input is assumed homogeneous. Then, the medium gradually becomes more 'transparent' due to burning out of the ^{64}Zn isotope. This isotope was excited predominantly because the laser frequency was detuned from the transition line of the ^{64}Zn isotope by 2.1 GHz and from the transition line of the ^{66}Zn isotope by 2.76 GHz (the width of the laser line was 500 MHz). The experimental conditions are listed below.

Radiation power/W 3
Degree of contamination of ^{66}Zn by ^{64}Zn and ^{67}Zn isotopes... 0.0099
Number of pulses during the flight time 500
Number of photons per atom of the ^{66}Zn isotope 20.0
Absorption of radiation in the active region (%)..... 52
Yield of the ^{66}Zn isotope (output-to-input flow ratio) (%)..... 31

Longitudinal gas circulation. The disadvantage of the transverse gas circulation is a strong inhomogeneous distribution of a residual amount of a burnt out isotope along the chamber axis. The longitudinal gas circulation does not have this disadvantage. Fig. 14 shows the distributions of two isotopes along the tube axis. The parameters of this regime are presented below.

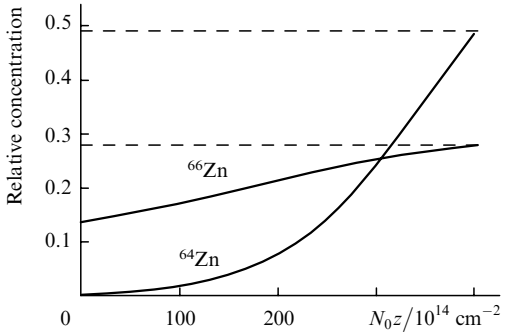

Figure 14. Spatial distribution of isotopes during the longitudinal gas circulation. Radiation is directed along the decreasing coordinate (dashed straight lines are concentrations of atoms in the absence of radiation.

Radiation power/W 2
Degree of contamination of ^{66}Zn by ^{64}Zn and ^{67}Zn isotopes.... 0.029
Number of pulses during the flight time 3100
Number of photons per atom of the ^{66}Zn isotope 6.75
Absorption of radiation in the active region (%)..... 71
Yield of the ^{66}Zn isotope (output-to-input flow ratio) (%)..... 49

The parameters of the method strongly depend on the detuning frequency. Fig. 15 shows the basic parameters of the isotope separation process upon the transverse gas circulation. One can see that the degree of contamination of the ^{66}Zn isotope by undesirable isotopes has a distinct minimum. This is explained by the fact that the excitation selectivity decreases at small detunings, while at large detunings the absorption of laser radiation decreases.

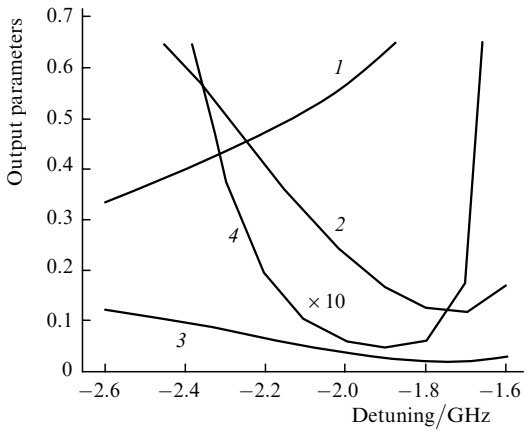

Figure 15. Main output parameters as functions of the detuning: total absorption (*1*); ratio of the output flow of ^{66}Zn to its input flow (*2*); yield of ^{66}Zn atoms per photon (*3*); degree of contamination of the ^{66}Zn isotope by ^{64}Zn and ^{68}Zn isotopes (*4*).

Thus, we have shown by the example of an 'inconvenient' element for laser isotope separation such as zinc that the method proposed by us has acceptable energy efficiency and can be quite competitive with other methods.

5.4 Experiments on separation of zinc isotopes

Zinc atoms were excited in the separation region along the gas flow at 307 nm at the intercombination $4s^2\,{}^1S_0 - 4p\,{}^3P_1^0$ transition by the second harmonic of the tunable dye laser described in Section 2. The average output power of the laser was ~ 2 W and the laser beam diameter was ~ 1 cm. The upper excited state used in the experiments had a comparatively long lifetime of 10.5 μs.

Figs 16 and 17 show the experimental and calculated absorption spectra at the resonance $4s^2\,{}^1S_0 \rightarrow 4p\,{}^3P_1^0$ transition for the main isotopes of zinc at 350 °C and the total absorption spectrum. Polyatomic oxygen-containing molecules of diethyl ether $(C_2H_5)O$ and methanol CH_3OH were used as a reagent gas. In this case, the reaction of excited atoms with reagent-gas molecules proceeds with the for-

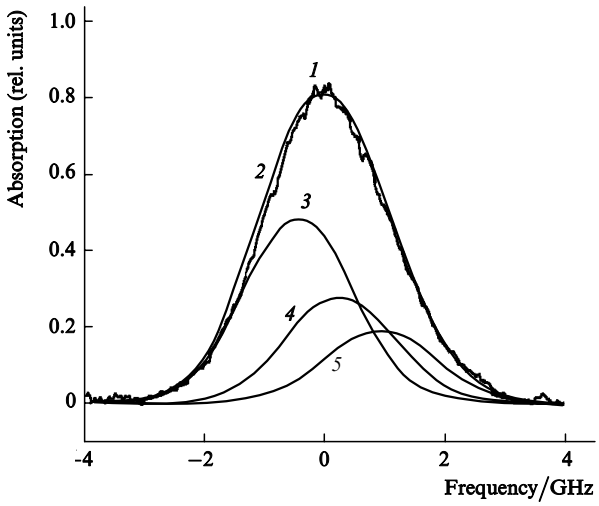

Figure 16. Absorption spectra of Zn at the $4s^2\,{}^1S_0 \rightarrow 4p\,{}^3P_1^0$ transition: (*1*) experiment; (*2*) calculation. Calculated absorption spectra of ^{64}Zn (*3*), ^{66}Zn (*4*), and ^{68}Zn (*5*) isotopes.

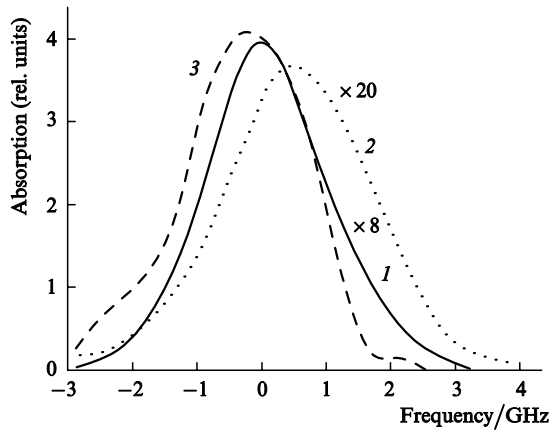

Figure 17. Absorption spectra of Zn in a collector chamber at the $4s^2\,{}^1S_0 \rightarrow 4p\,{}^3P_1^0$ transition recorded at the laser detuning from the centre by −2 GHz (*1*) and 2 GHz (*2*); (*3*) Doppler contour.

mation of a stable compound ZnO, which precipitates on the chamber walls in the separation region. The rate constant of the reaction of $Zn(4p\,{}^3P_1^0)$ with diethyl ether is $k^* = 1.61 \times 10^{-9}$ cm^3 s^{-1}, while the rate constant of the reaction with unexcited atoms is negligibly small ($k < 10^{-14}$ cm^3 s^{-1}).

When the laser was tuned to the centre of the Doppler line of zinc atoms, all the atoms in the collector chamber were virtually burnt out. This demonstrates efficient excitation of zinc atoms in the separation chamber and the efficiency of the chemical reaction. When the laser was detuned from the centre of the Doppler line, the absorption line was distorted, which was detected in the collector chamber with the help of a low-power laser. Fig. 17 shows the results of these experiments, which were performed at the atomic concentration $\sim 10^{13}$ cm^{-3} in the separation region.

When the laser was tuned from the line centre by −2 GHz, the maximum of the Doppler line shifted to the right. This is explained by predominant excitation and subsequent burning out of ^{64}Zn isotopes (Fig. 16). The opposite situation was observed when the laser was detuned by 2 GHz.

It follows also from Fig. 18 that the number of burnt out

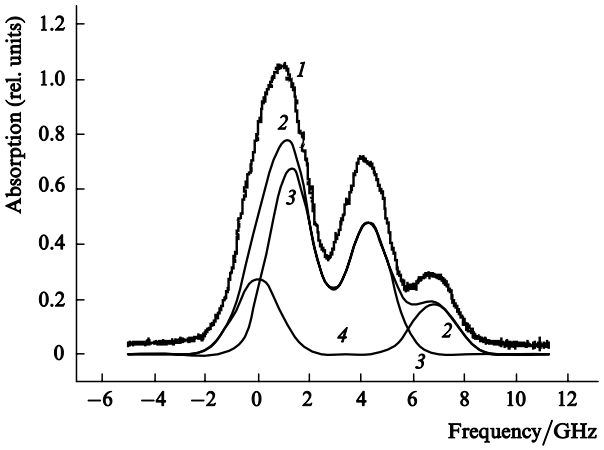

Figure 18. Absorption spectra of Rb at the $5S_{1/2} - 11P_{3/2}$ transition: (*1*) experiment; (*2*) calculation. Calculated absorption spectra of ^{85}Rb (*3*) and ^{87}Rb (*4*) isotopes.

atoms detected in the collector chamber exceeds the number of atoms excited in the separation chamber. This is related to the secondary reactions of formation of radicals with unexcited atoms.

Comparison of the experimental shift of the Doppler line with the calculation showed that more than 95 % of the ^{64}Zn isotope was burnt out in the separation chamber. The same results were obtained from mass-spectrometric analysis of zinc precipitated on the walls of the collector chamber. The production of the separated isotope was ~ 1 g during three-hour exposure and was determined by the flow rate of the working gas.

5.5 Separation of rubidium isotopes by exciting Rydberg states

The isotope enrichment method described in Section 5.4 can be applied to almost any atoms and molecules because they all have highly excited long-lived states. Below, we present the example of separation of isotopes of rubidium as a representative of elements with short-lived lower states.

Fig. 18 shows the absorption spectra of rubidium atoms in the separation chamber at the $5S_{1/2} - 11P_{3/2}$ Rydberg transition, which were recorded by measuring absorption or luminescence. In both cases, the spectra are identical. The spectra did not change up to pressures of ~ 5 Torr and the concentration of rubidium atoms $\sim 10^{13}$ cm^{-3}. The calculated absorption spectra well agree with the experimental spectra recorded at 120 °C. Also, the calculated absorption spectra of the individual hyperfine-structure components of the ^{85}Rb and ^{87}Rb isotopes are presented. Excitation of these isotopes through the hyper-fine structure components ($F = 1 \rightarrow F = 0$, 1, 2 for ^{87}Rb and $F = 2 \rightarrow F = 1$, 2, 3 for ^{85}Rb) features good selectivity. The long lifetime of the Rydberg state (0.5 μs under our experimental conditions) makes it possible to perform efficient chemical reactions.

Molecules of methanol CH_3OH and diethyl ether $(C_2H_5)_2O$ were used as a reagent gas. The rate constants k^* of reactions of these molecules with $Rb(11P_{3/2})$ were 1.47×10^{-9} and 8.4×10^{-10} cm^3 s^{-1}, respectively. The rate constant for unexcited rubidium atoms was more than three orders of magnitude lower. The isotope separation was performed at the reagent-gas pressure for which the lifetime of the $Rb(11P_{3/2})$ state was shorter than 50 ns. This allowed us to suppress completely superradiance and to use pump radiation most efficiently.

Fig. 19 shows the absorption spectra of rubidium atoms at concentration $\sim 10^{12}$ cm^{-3} at the $5S_{1/2} - 5P_{3/2}$ transition, which were detected at the end of the separation chamber. These spectra give information on the isotopic composition of rubidium atoms. The experimental results show that, when the laser is tuned to the absorption peak ($F = 1 \rightarrow F = 0$, 1, 2) of the ^{87}Rb isotope, the content of this isotope at the end of the separation chamber decreases below ~ 10 % of its initial amount. It is important to note that, when highly excited states are used, the rates of chemical reactions prove to be so high that isotope separation can be performed at a comparatively low pressure of the reagent gas (~ 1 Torr).

6. Conclusions

(1) It has been shown theoretically and experimentally that coherent two-photon excitation of atoms is promising for isotope separation. The isotope separation was performed

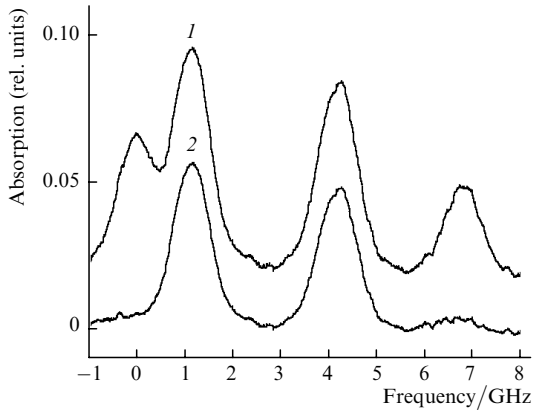

Figure 19. Absorption spectra of Rb at the $5S_{1/2} - 5P_{3/2}$ transition in the absence (*1*) and presence (*2*) of pump radiation.

by this method under conditions when the isotopic structure of spectral lines was within the Doppler contour. This allowed us to extend the number of elements that can be subjected to laser isotope separation, including elements whose isotopic structure is masked by the Doppler contour, in particular, Si and Zn atoms.

(2) The model was developed and a high efficiency of laser isotope separation in a gas flow was demonstrated by using photochemical reactions between atoms in long-lived states. The isotopes of Rb and Zn were separated.

(3) The efficiency of laser isotope separation by using rapid chemical reactions involving Rydberg atoms was demonstrated.

(4) The model of two-photon coherent excitation was developed, which takes into account cascade superluminescence, which are typical for isotope separation in weight amounts.

(5) The model was developed and the conditions for efficient removal of rare isotopes from a product are determined. A deep purification of lead from the radioactive ^{210}Pb isotope was performed.

(6) Based on physicochemical principles proposed and studied in the paper, a multifunctional unit for was developed and built for separation of weight amounts of isotopes of a variety of elements. Semicommercial units for isotope separation were built, which produce commercial isotopes [66, 67].

References

1. Letokhov V.S., Ambartzumian R.V. *IEEE J. Quantum Electron.*, **7**, 305 (1971).
2. Ambartzumian R.V., Letokhov V.S. *Appl. Opt.*, **11**, 354 (1972).
3. Ambartzumian R.V., Kalinin V.P., Letokhov V.S. *Pis'ma Zh. Eksp. Teor. Fiz.*, **13**, 305 (1971).
4. Letokhov V.S. *Science*, **180**, 451 (1973).
5. Letokhov V.S. *Opt. Commun.*, **7**, 59 (1973).
6. Karlov N.V., Prokhorov A.M. *Usp. Fiz. Nauk*, **118**, 583 (1976).
7. Letokhov V.S., Muhr B. *Kvantovaya Elektron.*, **3**, 248 (1976) [*Sov. J. Quantum Electron.*, **6**, 129 (1976)].
8. Letokhov V.S., Muhr B. *Kvantovaya Elektron.*, **3**, 485 (1976) [*Sov. J. Quantum Electron.*, **6**, 259 (1976)].
9. Basov N.G., Belenov E.M., Isakov V.A., Markin E.P., Oraevsky A.N., Romanenko V.I. *Usp. Fiz. Nauk*, **121**, 427 (1977).
10. Letokhov V.S., Mishin V.I., Puretsky A.A. *Khim. Plasm.* (3), 3 (Moscow: Atomizdat, 1977).
11. Karlov N.V. *Trudy FIAN*, **114**, 3 (1979).
12. Karlov N.V., Krynetskii B.B., Mishin V.A., Prokhorov A.M. *Usp. Fiz. Nauk*, **127**, 593 (1979).
13. Paisner J.A. *Appl. Phys. B*, **46**, 253 (1988).
14. Yakovlenko S.I. *Kvantovaya Elektron.*, **25**, 971 (1998) [*Quantum Electron.*, **28**, 945 (1998)].
15. Mishin V.A., in *Izotopy* (Isotopes), Baranov V.Yu. (Ed.) (Moscow: IZDAT, 2000) p. 308.
16. Isaev A.A., Kazaryan M.A., Petrash G.G. *Pis'ma Zh. Eksp. Teor. Fiz.*, **16**, 40 (1972).
17. Batenin V.M., Buchanov V.V., Kazaryan M.A., Klimovskii I.I., Molodykh E.I. *Lazery na samoogranichennykh perekhodakh atomov metallov* (Self-Contained Metal Atom Lasers) (Moscow: Nauchnaya Kniga, 1998).
18. Little C.E. *Metal Vapour Lasers* (New York, John Wiley&Sons, 1999).
19. Devis J., Devis R. Laser isotope separation program-8.1 Overview, in Laser Program Annual Report-1976, UCRL-50021-76, Lawrence Livermore National Laboratory, CA, 8/3-8 (June 1977).
20. Spaeth M. Laser isotope separation program-8.1 Overview, in Laser Program Annual Report-1976, UCRL-50021-76, CA, 8/29-33 (June 1977).
21. Shirayama S., Ueda H., Mikatsura T., Konagai Ch. *Proc. SPIE Int. Soc. Opt. Eng.*, **1225**, 279 (1990).
22. Morioka N. *Proc. SPIE Int. Soc. Opt. Eng.*, **1859**, 2 (1993).
23. Camarcat N., Lafon A., Perves J., Rosengard A. *Proc. SPIE Int. Soc. Opt. Eng.*, **1859**,14 (1993).
24. Haynam C.A., Comaskey B.J., Conway J., Eggert J., Glaser J., Ng E.W., Paisner J.A., Solarz R.W., Worden E.F. *Proc. SPIE Int. Soc. Opt. Eng.*, **1859**, 24 (1993).
25. Bettinger A., Neu M., Maury J., Chatelet J.A. *Proc. SPIE Int. Soc. Opt. Eng.*, **1859**, 108 (1993).
26. Forest G. *Laser Focus*, **22** (4), 23 (1986).
27. Kiernan V. *Laser Focus World*, **33** (10), 78 (1977).
28. Grant B. *Photon. Spectra*, **31** (10), 46 (1997).
29. Demidova N.S., Mishin V.A. *Pis'ma Zh. Tekh. Fiz.*, **23**, 42 (1977).
30. Borisov S.K., Kuz'mina M.A., Mishin V.A. *Dokl. III Vseros. Nauchnoi konf. 'Fiziko-khimicheskie protsessy pri selektsii atomov i molekul* (Proc. III All-Russian Conference on Physicochemical Processes in Selection of Atoms and Molecules) (Zvenigorod, Moscow; TSNIIatominform, 1988) p. 40.
31. Buchanov V.V., Kazaryan M.A, Kalugin M.M., Prokhorov A.M. *Laser Phys.*, **11**, 1332 (2001).
32. Buchanov V.V., Kazaryan M.A., Kalugin M.M., Prokhorov A.M. *Dokl. V Vseros. (mezhdunarodnoi) nauchnoi konf. 'Fiziko-khimicheskie protsessy pri selektsii atomov i molekul'* (Proc. V All-Russian International Conference on Physicochemical Processes in Selection of Atoms and Molecules) (Zvenigorod, Moscow; TSNIIatominform, 2001) p. 111.
33. Buchanov V.V., Kazaryan M.A, Kalugin M.M., Prokhorov A.M. *Tech. Digest of Intern. Conf. Lasers'2001* (Tucson, Arizona, 2001) p. 34.
34. Grove R.E. Copper vapour laser overview, Laser program annual report-1979 (LLNL: Livermore, CA), 9-4 to 9-5 (1980).
35. Devis J.L., Shore B.W. Technical and systems highlights, Laser program annual report-1980 (LLNL: Livermore, CA), 10-13 to 10-17, UCRL-5002180 (1981).
36. Warner B.E. *Tech. Digest Opt. Soc. Am.* (Wasington, DC, 516-18, 1991).
37. Kearsley A. *Proc. SPIE Int. Soc. Opt. Eng.*, **1225**, 270 (1990).
38. Sabotinov N.V., Vuchkov N.K., Asadjov D.N. *Proc. SPIE Int. Soc. Opt. Eng.*, **1225**, 289 (1990).
39. Bass I.L., Bonanno R.E., Hackel R.P., Hammond P.R. *Appl. Opt.*, **31**, 6993 (1992).
40. Doizi D., in *Pulsed Metal Vapour Lasers* (Dordrcht, Kluwer Academic Publishers, 1996) p. 303.
41. Vasil'ev S.V., Mishin V.A., Shavrova T.V. *Kvantovaya Elektron.*, **24**, 131 (1997) [*Quantum Electron.*, **27**, 126 (1997)].
42. Tabata Y., Hara K., Ueguri S. *Proc. SPIE Int. Soc. Opt. Eng.*, **1628**, 32 (1992).

43. Lyabin N.A., Chursin A.D., Ugol'nikov S.A., Koroleva M.E., Kazaryan M.A. *Kvantovaya Elektron*., **31**, 191 (2001) [*Quantum Electron*., **31**, 191 (2001)].
44. Bokhan P.A., Buchanov V.V., Zakrevskii D.E., Stepanov A.Yu., Fateev N.V. *Pis'ma Zh. Eksp. Teor. Fiz*., **71**, 705 (2000).
45. Bokhan P.A., Buchanov V.V., Zakrevskii D.E., Stepanov A.Yu., Fateev N.V. *Dokl. IV Vseros. (mezhdunarodnoi) nauchnoi konf. 'Fiziko-khimicheskie protsessy pri selektsii atomov i molekul'* (Proc. IV All-Russian International Conference on Physicochemical Processes in Selection of Atoms and Molecules) (Zvenigorod, Moscow; TSNIIatominform, 2000) p. 106.
46. Lyabin N.A. *Opt. Atmos. Okean*., **13**, 258 (2000).
47. Maximov O.P., Mishin V.A., Mashkunov A.G., et al. *Techn. Didest of Intern. Conf. Lasers'97* (New-Orlean, Lousiana, McLEAN, 1997).
48. Bokhan P.A., Zakrevskii D.E., Kochubei S.A., Stepanov A.Yu., Fateev N.V. *Kvantovaya Elektron*., **31**, 132 (2001) [*Quantum Electron*., **31**, 132 (2001)].
49. Moshkunov A.I., Zakrevskii D.E., Rakhimov G.G., Yudin N.A. *Dokl. IV Vseros. (mezhdunarodnoi) nauchnoi konf. 'Fiziko-khimicheskie protsessy pri selektsii atomov i molekul'* (Proc. IV All-Russian International Conference on Physicochemical Processes in Selection of Atoms and Molecules) (Zvenigorod, Moscow; TSNIIatominform, 2000) p. 102.
50. Anderson S.G. *Laser Focus World*, **37** (1), 88 (2001).
51. Kobtsev S.M., Korablev A.V., Kukarin S.V., Sorokin V.B. *Proc. SPIE Int. Soc. Opt. Eng*., **4353**, 189 (2001).
52. Bokhan P.A., Zakrevskii D.E., Stepanov A.Yu., Fateev N.V. *Dokl. V Vseros. (mezhdunarodnoi) nauchnoi konf. 'Fiziko-khimicheskie protsessy pri selektsii atomov i molekul'* (Proc. V All-Russian International Conference on Physicochemical Processes in Selection of Atoms and Molecules) (Zvenigorod, Moscow; TSNIIatominform, 2001) p. 60.
53. Bokhan P.A., Zakrevskii D.E., Kim V., Fateev N.V. *Dokl. V Vseros. (mezhdunarodnoi) nauchnoi konf. 'Fiziko-khimicheskie protsessy pri selektsii atomov i molekul'* (Proc. V All-Russian International Conference on Physicochemical Processes in Selection of Atoms and Molecules) (Zvenigorod, Moscow; TSNIIatominform, 2001) p. 61.
54. Greenland P.T. *Contemporary Phys*., **31**, 405 (1990).
55. Bokhan P.A., Buchanov V.V., Zakrevskii D.E., Stepanov A.Yu. *Dokl. IV Vseros. (mezhdunarodnoi) nauchnoi konf. 'Fiziko-khimicheskie protsessy pri selektsii atomov i molekul'* (Proc. IV All-Russian Conference on Physicochemical Processes in Selection of Atoms and Molecules) (Zvenigorod, Moscow; TSNIIatominform, 1999) p. 86.
56. Borisov S.K., Kuz'mina M.A., Mishin V.A. *Kvantovaya Elektron*., **22**, 722 (1995) [*Quantum Electron*., **25**, 695 (1995)].
57. Borisov S.K., Mishin V.A. *Trudy IOFAN*, **24**, 3 (1990).
58. Allen L., Eberly J.H. *Optical Resonance and Two-Level Atoms* (New York: Wiley, 1975; Moscow: Mir, 1978).
59. Salomon E.B. *Spectrochim. Acta*, **45B**, N 1,2, 37 (1990).
60. Grogor'ev I.S., Meilikhov E.Z. (Eds) *Fizicheskie velichiny. Spravochnik* (Handbook of Physical Quantities) (Moscow: Energoizdat, 1991).
61. Landau L.D., Lifshits E.M. *Kvantovaya Mekhanika* (Quantum Mechanics) (Moscow: Nauka, 1974).
62. Sobel'man I.I. *Vvedenie v teoriyu atomnykh spektrov* (Introduction to the Theory of Atomic Spectra) (Moscow: Fizmatlit, 1963).
63. Getty E.T. *Appl. Phys. Lett*., **7**, 6 (1965).
64. Khanin Ya.I. *Dinamika kvantovykh generatorov* (Dynamics of Lasers) (Moscow: Sov. Radio, 1975).
65. Smirnov B.M. *Vozbuzhdennye atomy* (Excited Atoms) (Moscow: Energoizdat, 1982).
66. Bokhan P.A. *Dokl. IV Vseros. (mezhdunarodnoi) nauchnoi konf. 'Fiziko-khimicheskie protsessy pri selektsii atomov i molekul'* (Proc. IV All-Russian Conference on Physicochemical Processes in Selection of Atoms and Molecules) (Zvenigorod, Moscow; TSNIIatominform, 1999) p. 115.
67. Bokhan P.A., Zakrevskii D.E., Stepanov A.Yu., Fateev N.V. *Dokl. V Vseros. (mezhdunarodnoi) nauchnoi konf. 'Fiziko-khimicheskie protsessy pri selektsii atomov i molekul'* (Proc. V All-Russian International Conference on Physicochemical Processes in Selection of Atoms and Molecules) (Zvenigorod, Moscow; TSNIIatominform, 2000) p. 106.